Article:
Lesnic, D and Alosaimi, M (2023) Determination of the space-dependent source in the thermal-wave model of bio-heat transfer. Computers and Mathematics with Applications, 129. pp. 34-49. ISSN: 0898-1221

https://doi.org/10.1016/j.camwa.2022.10.026

Determination of a space-dependent source in the thermal-wave model of bio-heat transfer

M. Alosaimi[1,2] and D. Lesnic[1,*]
[1] *Department of Applied Mathematics, University of Leeds, Leeds LS2 9JT, UK*
[2] *Department of Mathematics and Statistics, College of Science, Taif University, P.O. Box 11099, Taif 21944, Saudi Arabia*
E-mails: mmmaal@leeds.ac.uk (M. Alosaimi), amt5ld@maths.leeds.ac.uk (D. Lesnic* corresponding author)

Abstract. We consider linear but ill-posed inverse problems consisting of finding the unknown space-dependent source in the thermal-wave model of bio-heat transfer from final-time or time-average temperature measurements. In contrast to the previous research on parabolic bio-heat transfer models, this work concerns a more involved and practical hyperbolic model used in biomedical engineering. First, the unique solvability of the inverse source linear problems is established. Then, the inverse problems are recast as variational problems, allowing the gradients of the least-squares objective functionals to be derived. These later problems are solved iteratively using the conjugate gradient method combined with the discrepancy principle. Finally, the inversion algorithm is tested on identifying one- and two-dimensional space-dependent sources.

Keywords: Inverse source problem; bio-heat transfer; conjugate gradient method; regularization; thermal-wave model

1. Introduction

Abnormalities associated with biological tissues, such as tumour formation, have a major impact on organs malfunctioning. Therefore, these disorders must be detected and treated early to save lives and improve the general health. To this end, several therapeutic interventions guided by medical imaging have been successfully discovered and developed, e.g. hyperthermia and cryoablation treatments. For instance, in hyperthermia, tumours are destroyed by increasing their temperature to about 42–46°C, while keeping the healthy tissues undamaged [6, 29]. Optimizing the medical treatment, e.g. by regulating the tissue temperature, is significant. Loulou and Scott [22] proposed such a method to determine the optimal heating applied to reach the thermal dose required for cancer eradication. Other applications include determining the time it would take to eliminate tumours [28], evaluating the thermal response of biological tissues to medical treatment [17], and finding the thermo-physical properties of biological tissues [3, 4].

Mathematical bio-heat transfer models have been the basis of the above-mentioned applications. The Pennes' bio-heat parabolic model [26] has been the most widely used in the literature despite its unphysical assumption of instantaneous heat propagation. This is resolved by the hyperbolic thermal-wave model of bio-heat transfer [20], as it accounts for the finite speed of thermal propagation.

Inverse problems of identifying the source from different types of measurements, e.g.

boundary, integral or nonlocal, have been extensively studied in the past. Such problems arise in many areas of engineering and applied sciences, e.g. tsunami source reconstruction and pollutant source detection. Hasanov [13], for example, investigated the possibility of determining the sources in the wave equation and in a Neumann boundary condition from additional terminal data. Nguyen [24] used a quasi-reversibility method to numerically reconstruct the space-dependent source in hyperbolic equations from lateral Cauchy data, whilst Romanov and Hasanov [27] investigated the same retrieval but from final-time measurement. Lesnic et al. [19] developed the Landweber method and conjugate gradient method (CGM) to numerically identify the space-dependent source in the wave equation from upper-base or time-average displacement measurements. Inverse problems of determining the space- and time-dependent source have also been investigated in the literature, e.g. [11, 12] for parabolic equations and [2] for hyperbolic equations. Recently, Hào et al. [12] proved the convergence of a Crank-Nicolson Galerkin method for the reconstruction of such a missing source in parabolic equations from a partial boundary observation.

Inverse bio-heat transfer problems have also been formulated and investigated using various approaches. Bazán et al. [7] used the pseudo-spectral collocation method coupled with the regularized Gauss–Newton method to identify the space-dependent perfusion coefficient in the two-dimensional Pennes' bio-heat equation. Jalali et al. [14] used the CGM to simultaneously reconstruct the time-dependent source and the heat transfer coefficient during the hyperthermal treatment of a single-layered tissue. Cao and Lesnic [9] developed and implemented the CGM to identify the space-dependent perfusion coefficient in the Pennes' bio-heat equation from time-average or upper-base temperature measurements. Baghban and Ayani [6] utilized a sequential method to numerically recover the time-dependent source applied to a multi-layered tissue from skin temperature measurement.

Despite much research in inverse source problems for the parabolic bio-heat equation, only a few authors have looked at solving their counterpart for hyperbolic models. For instance, in [23], the authors used variational and spectral methods to prove the uniqueness of the solution of the inverse space-dependent source problem for the time-fractional dual-phase-lag model from a measured final-time observation. In this paper, we first establish the unique solvability of the inverse problems of estimating the space-dependent source in the thermal-wave model of bio-heat transfer from final-time or time-average temperature measurements as additional information using the method of separation of variables similar to the analysis of [8] for the wave equation. Afterwards, the CGM is employed to numerically solve the linear but ill-posed inverse space-dependent source problems for the thermal-wave bio-heat transfer model.

This paper is structured as follows. Section 2 describes the mathematical formulation of the inverse space-dependent source problems. In Section 3, the inverse problems are reformulated as variational problems, and the least-squares objective functionals are proved Fréchet differentiable and explicit formulae for their gradients are derived. The CGM is then described for the minimization of the objective functionals. In Section 4, numerical results concerning identifying one- and two-dimensional space-dependent sources exhibiting different behaviours are presented and discussed. Finally, Section 5 highlights the conclusions of

the work.

2. Mathematical formulation

Let $\Omega \subset \mathbb{R}^d, d = 1, 2, 3$, be a bounded domain with a piecewise smooth boundary $\partial\Omega$. The heat propagation in biological bodies is governed by the thermal-wave model of bio-heat transfer given by, [21],

$$\rho_{\mathrm{t}} c_{\mathrm{t}} \overline{\tau} \frac{\partial^2 T}{\partial \bar{t}^2} + (\rho_{\mathrm{t}} c_{\mathrm{t}} + \overline{\tau} \rho_b c_b w_b) \frac{\partial T}{\partial \bar{t}} = k \nabla^2 T + \rho_b c_b w_b (T_a - T) + Q_m + Q_e + \overline{\tau} \frac{\partial}{\partial \bar{t}} (Q_m + Q_e), \quad (\bar{\mathbf{x}}, \bar{t}) \in \Omega \times (0, t_{\mathrm{f}}], \tag{1}$$

where $T, \rho_{\mathrm{t}}, c_{\mathrm{t}}$ and k represent the temperature [°C], density [kg/m^3], specific heat [J/(kg °C)] and thermal conductivity [W/(m °C)] of the tissue, respectively, ρ_b, c_b and w_b stand for the density [kg/m^3], specific heat [J/(kg °C)] and perfusion rate [s^{-1}] of the blood, respectively, $\overline{\tau}$ is the relaxation time [s] required for the thermal waves to propagate, T_a is the (arterial) blood temperature [°C], Q_m and Q_e are heat generations [W/m^3] due to metabolism and external heating, respectively, t_{f} is the duration of the thermal process [s], $\bar{\mathbf{x}}$ is the space position vector with components measured in [m], and $\bar{t}$ is the time [s].

Equation (1) is considered subject to the initial conditions

$$T|_{\bar{t}=0} = T_0, \quad \left.\frac{\partial T}{\partial \bar{t}}\right|_{\bar{t}=0} = 0 \quad \text{in } \Omega, \tag{2}$$

and the temperature specification Dirichlet boundary condition

$$T|_{\partial\Omega \times [0, t_{\mathrm{f}}]} = \mathrm{f} \quad \text{on } \partial\Omega \times [0, t_{\mathrm{f}}], \tag{3}$$

assuming also the compatibility condition $\mathrm{f}|_{\partial\Omega \times \{0\}} = T_0|_{\partial\Omega}$. Instead of (3), adiabatic or Robin boundary conditions can also be considered.

The direct problem concerns finding T satisfying (1)–(3) when the source Q_e and/or Q_m are/is known. However, if the source Q_e and/or Q_m cannot be directly observed and is therefore unknown, the problem becomes an inverse problem of determining the temperature T and the source satisfying (1)–(3) alongside additional data. Such data may be the measurement of the temperature T at the final time $t = t_{\mathrm{f}}$, namely,

$$T(\bar{\mathbf{x}}, t_{\mathrm{f}}) = T_{t_{\mathrm{f}}}(\bar{\mathbf{x}}), \quad \bar{\mathbf{x}} \in \Omega, \tag{4}$$

or the average temperature

$$\int_0^{t_{\mathrm{f}}} T(\bar{\mathbf{x}}, \bar{t}) d\bar{t} = \mathcal{T}_{t_{\mathrm{f}}}(\bar{\mathbf{x}}), \quad \bar{\mathbf{x}} \in \Omega. \tag{5}$$

Measurement (5) is preferred in case the measurement (4) is too noisy. In this paper, we investigate the spatial dependence of the governing equation (1) in case of the slab $\Omega = [0, L_1]$ in one-dimension $d = 1$ and the rectangle $\Omega = [0, L_1] \times [0, L_2]$ in two-dimensions $d = 2$, where

$L_1 > 0$ and $L_2 > 0$ stand for the depth and width of the tissue, respectively.

In the following section, the thermal-wave model of bio-heat transfer (1)–(3) in two-dimensions $d = 2$ is non-dimensionalized.

2.1 Dimensionless model

Consider the thermal-wave model of bio-heat transfer (1)–(3) in two-dimensions $d = 2$ and use the following non-dimensionalization:

$$\begin{aligned} x_1 = \frac{\bar{x}_1}{L_1}, \quad x_2 = \frac{\bar{x}_2}{L_2}, \quad (t, \tau) = \frac{1}{t_{\mathrm{f}}}(\bar{t}, \bar{\tau}), \quad \theta = \frac{T - T_0}{T_0}, \\ \theta_a = \frac{T_a - T_0}{T_0}, \quad f = \frac{\mathrm{f} - T_0}{T_0}, \quad F = \frac{(Q_e + Q_m)t_{\mathrm{f}}^2}{\tau T_0 C_{\mathrm{t}}}, \end{aligned} \tag{6}$$

where $\bar{\mathbf{x}} = (\bar{x}_1, \bar{x}_2)$, $C_{\mathrm{t}} = \rho_{\mathrm{t}} c_{\mathrm{t}}$ is the heat capacity of the tissue, and the initial temperature T_0 has been assumed uniform and equal to a non-zero constant. Then, the dimensionless version of the thermal-wave model (1)–(3) is

$$\begin{aligned} \frac{\partial^2 \theta}{\partial t^2} + a_1 \frac{\partial \theta}{\partial t} = a_2 \frac{\partial^2 \theta}{\partial x_1^2} + a_3 \frac{\partial^2 \theta}{\partial x_2^2} - a_4(\theta - \theta_a) + F + \tau \frac{\partial F}{\partial t}, \\ \mathbf{x} = (x_1, x_2) \in (0,1)^2, \quad t \in (0,1], \end{aligned} \tag{7}$$

subject to the initial conditions

$$\theta(x_1, x_2, 0) = 0, \qquad \frac{\partial \theta}{\partial t}(x_1, x_2, 0) = 0, \quad (x_1, x_2) \in [0,1]^2, \tag{8}$$

and the Dirichlet boundary condition

$$\theta(x_1, x_2, t) = f(x_1, x_2, t), \quad (x_1, x_2, t) \in \partial(0,1)^2 \times [0,1], \tag{9}$$

satisfying $f(x_1, x_2, 0) = 0$ for $(x_1, x_2) \in \partial[0,1]^2$, where:

$$a_1 = \frac{t_{\mathrm{f}}}{\overline{\tau}} + \frac{w_b C_b t_{\mathrm{f}}}{C_{\mathrm{t}}}, \quad a_2 = \frac{k t_{\mathrm{f}}^2}{\overline{\tau} C_{\mathrm{t}} L_1^2}, \quad a_3 = \frac{k t_{\mathrm{f}}^2}{\overline{\tau} C_{\mathrm{t}} L_2^2}, \quad a_4 = \frac{w_b C_b t_{\mathrm{f}}^2}{\overline{\tau} C_{\mathrm{t}}}, \tag{10}$$

where $C_b = \rho_b c_b$ is the heat capacity of the blood. In the above non-dimensional form, equations (4) and (5) can be written as

$$\theta(\mathbf{x}, 1) = \frac{T_{t_{\mathrm{f}}}(\mathbf{x}) - T_0}{T_0} =: \theta_1(\mathbf{x}), \quad \mathbf{x} \in (0,1)^2, \tag{11}$$

and

$$\int_0^1 \theta(\mathbf{x}, t) dt = \frac{\mathcal{T}_{t_{\mathrm{f}}}(\mathbf{x})}{T_0 t_{\mathrm{f}}} - 1 =: \Theta_1(\mathbf{x}), \quad \mathbf{x} \in (0,1)^2. \tag{12}$$

Remark 2.1.1. *We remark that through the change of variables:*

$$\theta(\mathbf{x}, t) = e^{-a_1 t/2} U(\mathbf{x}, t), \quad (\mathbf{x}, t) \in [0,1]^3, \tag{13}$$

the model (7)–(9) *becomes:*

$$\frac{\partial^2 U}{\partial t^2} = a_2 \frac{\partial^2 U}{\partial x_1^2} + a_3 \frac{\partial^2 U}{\partial x_2^2} + \left(\frac{a_1^2}{4} - a_4\right) U + \left(a_4 \theta_a + F + \tau \frac{\partial F}{\partial t}\right) e^{a_1 t/2},$$
$$(x_1, x_2) \in (0,1)^2,\ t \in (0,1], \tag{14}$$

$$U(x_1, x_2, 0) = 0, \quad \frac{\partial U}{\partial t}(x_1, x_2, 0) = V_0(x_1, x_2), \quad (x_1, x_2) \in [0,1]^2, \tag{15}$$

$$U(x_1, x_2, t) = e^{a_1 t/2} f(x_1, x_2, t), \quad (x_1, x_2, t) \in \partial(0,1)^2 \times [0,1]. \tag{16}$$

There are two inverse problems, namely (7)–(9), (11) and (7)–(9), (12), termed IP1 and IP2, respectively, which we shall consider.

If $F = F(\mathbf{x}, t)$ depends on both space and time we obviously have non-uniqueness, but when $F = F(\mathbf{x})$ is independent of t, equation (7) simplifies to

$$\frac{\partial^2 \theta}{\partial t^2} + a_1 \frac{\partial \theta}{\partial t} = a_2 \frac{\partial^2 \theta}{\partial x_1^2} + a_3 \frac{\partial^2 \theta}{\partial x_2^2} - a_4(\theta - \theta_a) + F(\mathbf{x}),$$
$$\mathbf{x} = (x_1, x_2) \in (0,1)^2,\ t \in (0,1], \tag{17}$$

and we have the following uniqueness result.

Theorem 2.1. *If*

$$\frac{|C_{\mathrm{t}} - w_b C_b \overline{\tau}|}{\sqrt{\overline{\tau} C_{\mathrm{t}} k}} < 2\pi \sqrt{\frac{1}{L_1^2} + \frac{1}{L_2^2}} \tag{18}$$

then the inverse source problems IP1 and IP2 have at most one solution.

Proof. Let $\big(\theta_1(x_1, x_2, t), F_1(x_1, x_2)\big)$ and $\big(\theta_2(x_1, x_2, t), F_2(x_1, x_2)\big)$ be two solutions of the inverse problems associated with (8), (9), (17) and (11) or (12). Denote $\theta := \theta_1 - \theta_2$ and $F := F_1 - F_2$. Then, $\big(\theta(x_1, x_2, t), F(x_1, x_2)\big)$ satisfies

$$\frac{\partial^2 \theta}{\partial t^2} + a_1 \frac{\partial \theta}{\partial t} = a_2 \frac{\partial^2 \theta}{\partial x_1^2} + a_3 \frac{\partial^2 \theta}{\partial x_2^2} - a_4 \theta + F(x_1, x_2), \quad (x_1, x_2) \in (0,1)^2,\ t \in (0,1], \tag{19}$$

$$\theta(x_1, x_2, 0) = \frac{\partial \theta}{\partial t}(x_1, x_2, 0) = 0, \quad (x_1, x_2) \in [0,1]^2, \tag{20}$$

$$\theta(x_1, x_2, t) = 0, \quad (x_1, x_2, t) \in \partial(0,1)^2 \times [0,1], \tag{21}$$

$$\theta(x_1, x_2, 1) = 0, \quad (x_1, x_2) \in (0,1)^2, \tag{22}$$

or

$$\int_0^1 \theta(x_1, x_2, t) dt = 0, \quad (x_1, x_2) \in (0,1)^2. \tag{23}$$

Differentiate equation (19) with respect to t to eliminate the unknown source F and obtain

$$\theta_{ttt} + a_1 \theta_{tt} = a_2 \theta_{x_1 x_1 t} + a_3 \theta_{x_2 x_2 t} - a_4 \theta_t. \tag{24}$$

Seek the general solution of the above third-order linear PDE using the method of separation of variables as

$$\theta(x_1, x_2, t) = X(x_1) Y(x_2) Z(t).$$

This gives

$$\frac{Z''' + a_1 Z'' + a_4 Z'}{Z'} = \frac{a_2 X''}{X} + \frac{a_3 Y''}{Y} = -\mu^2, \tag{25}$$

for some constant μ. From the above expression, we obtain

$$\frac{a_2 X''}{X} = -\left(\mu^2 + \frac{a_3 Y''}{Y}\right) = -\lambda^2, \tag{26}$$

for some constant λ. The above expression gives the ODEs

$$X'' + \frac{\lambda^2}{a_2} X = 0 \quad \text{and} \quad Y'' + \frac{p^2}{a_3} Y = 0, \tag{27}$$

where $p^2 = \mu^2 - \lambda^2$. The homogeneous Dirichlet boundary conditions (21) gives $\lambda_n^2 = (n\pi)^2 a_2$ and $p_m^2 = (m\pi)^2 a_3$, and $X_n(x_1) = \sin(n\pi x_1)$ for $n \in \mathbb{N}^*$ and $Y_m(x_2) = \sin(m\pi x_2)$ for $m \in \mathbb{N}^*$. Also, denoting $Z'(t) = R(t)$, from (25) we have

$$R'' + a_1 R' + (a_4 + (n\pi)^2 a_2 + (m\pi)^2 a_3) R = 0. \tag{28}$$

The discriminant of the characteristic equation can be written as

$$\begin{aligned} \Delta_{n,m} &= a_1^2 - 4\big[a_4 + (n\pi)^2 a_2 + (m\pi)^2 a_3\big] \\ &= \frac{t_{\mathrm{f}}^2}{\overline{\tau} C_{\mathrm{t}}} \left\{ \frac{(C_{\mathrm{t}} - w_b C_b \overline{\tau})^2}{\overline{\tau} C_{\mathrm{t}}} - 4k \left[\left(\frac{n\pi}{L_1}\right)^2 + \left(\frac{m\pi}{L_2}\right)^2 \right] \right\}, \quad n, m \in \mathbb{N}^*. \end{aligned} \tag{29}$$

Under the assumption (18) we have that $\Delta_{n,m} < 0$ for all n, $m \in \mathbb{N}^*$. Then the general solution of the second-order ODE (28) is

$$Z'_{n,m}(t) = R_{n,m}(t) = e^{-a_1 t/2}\big[A_{n,m}\cos(\omega_{n,m} t) + B_{n,m}\sin(\omega_{n,m} t)\big], \tag{30}$$

where $A_{n,m}$ and $B_{n,m}$ are coefficients to be determined and $\omega_{n,m} = \dfrac{1}{2}\sqrt{-\Delta_{n,m}}$ for $n, m \in \mathbb{N}^*$. From the initial conditions (20) we have that

$$Z_{n,m}(0) = Z'_{n,m}(0) = 0.$$

Imposing $Z'_{n,m}(0) = 0$ yields $A_{n,m} = 0, \forall n, m \in \mathbb{N}^*$, and then (30) simplifies to

$$Z'_{n,m}(t) = B_{n,m} e^{-a_1 t/2} \sin(\omega_{n,m} t).$$

Integrating from 0 to t yields

$$\begin{aligned} Z_{n,m}(t) &= B_{n,m} \int_0^t e^{-a_1 \zeta/2} \sin(\omega_{n,m}\zeta) d\zeta \\ &= -\frac{2B_{n,m}[2\omega_{n,m} e^{-a_1 t/2}\cos(\omega_{n,m} t) + a_1 e^{-a_1 t/2}\sin(\omega_{n,m} t) - 2\omega_{n,m}]}{a_1^2 + 4\omega_{n,m}^2}, \quad n, m \in \mathbb{N}^*. \end{aligned}$$

Denote

$$\rho_{n,m}(t) \coloneqq 1 - e^{-a_1 t/2}\left(\cos(\omega_{n,m}t) + \frac{a_1}{2\omega_{n,m}}\sin(\omega_{n,m}t)\right).$$

Then, since

$$e^{a_1/2} \geq 1 + \frac{a_1}{2} > \cos(\omega_{n,m}) + \frac{a_1}{2}\frac{\sin(\omega_{n,m})}{\omega_{n,m}}$$

it follows that $\rho_{n,m}(1) > 0, \forall n, m \in \mathbb{N}^*$. Then, for the measurement (21) it follows that

$$0 = \theta(x_1, x_2, 1) = \sum_{n,m=1}^{\infty} \frac{B_{n,m}\rho_{n,m}(1)\omega_{n,m}}{a_1^2 + 4\omega_{n,m}^2}\sin(n\pi x_1)\sin(m\pi x_2).$$

This yields $B_{n,m} = 0, \forall n, m \in \mathbb{N}^*$. Hence, $\theta \equiv 0$. Also, from (19) it follows that $F \equiv 0$. Hence, uniqueness of solution holds.

Similarly, for the time-average measurement (23) we get

$$0 = \int_0^1 \theta(x_1, x_2, t)dt = \sum_{n,m=1}^{\infty} \frac{B_{n,m}\xi_{n,m}\omega_{n,m}}{a_1^2 + 4\omega_{n,m}^2}\sin(n\pi x_1)\sin(m\pi x_2),$$

where $\xi_{n,m} = \int_0^1 \rho_{n,m}(t)dt > 0$ since, based on

$$e^{a_1 t/2} \geq 1 + \frac{a_1 t}{2} > \cos(\omega_{n,m}t) + \frac{a_1 t}{2}\frac{\sin(\omega_{n,m}t)}{\omega_{n,m}t}, \quad \forall t \in (0, 1],$$

$\rho_{n,m}(t) > 0$ for $t \in (0, 1]$, and uniqueness follows from the same argument.

Remark 2.1. *If the boundary $\partial\Omega$ is insulated, then the Dirichlet boundary condition* (9) *is replaced by the adiabatic zero Neumann boundary condition*

$$\frac{\partial\theta}{\partial\boldsymbol{\nu}}(x_1, x_2, t) = 0 \quad \textit{for } (x_1, x_2, t) \in \partial\Omega \times \partial[0, 1]^2 \times (0, 1), \tag{31}$$

where $\boldsymbol{\nu}$ is the outward unit normal to the boundary. Then, the previous analysis modifies to give $\lambda_n^2 = (n\pi)^2 a_2$ and $X_n(x_1) = \cos(n\pi x_1)$ for $n \in \mathbb{N}$, and $p_m^2 = (m\pi)^2 a_3$ and $Y_m(x_2) = \cos(m\pi x_2)$ for $m \in \mathbb{N}$. We also obtain that
$Z'_{n,m}(t) = R_{n,m}(t) = B_{n,m}e^{-a_1 t/2}\sin(\omega_{n,m}t)$ for $(n, m) \in \mathbb{N}^2 \setminus \{(0, 0)\}$, $R_{0,0}(t) = C_1 e^{\lambda_+ t} + C_2 e^{\lambda_- t}$, where $\lambda_\pm = \frac{t_f}{2\overline{\tau}C_t}[-(C_t + w_b C_b\overline{\tau}) \pm |C_t - w_b C_b\overline{\tau}|]$. Observe that $\lambda_- < \lambda_+ < 0$. Since $Z'_{0,0}(0) = R_{0,0}(0) = 0$ it follows that $C_2 = -C_1$ hence $R_{0,0}(t) = C_1\big(e^{\lambda_+ t} - e^{\lambda_- t}\big)$.
Also,

$$Z_{0,0}(t) = B_{0,0}\int_0^t R_{0,0}(\tau)d\tau = B_{0,0}\left(\frac{e^{\lambda_+ t} - 1}{\lambda_+} - \frac{e^{\lambda_- t} - 1}{\lambda_-}\right),$$

where we have redenoted C_1 by $B_{0,0}$. Then,

$$\theta(x_1, x_2, t) = Z_{0,0}(t) + \sum_{(n,m)\in\mathbb{N}^2\setminus(0,0)} \frac{B_{n,m}\rho_{n,m}(t)\omega_{n,m}}{a_1^2 + 4\omega_{n,m}^2}\cos(n\pi x_1)\cos(m\pi x_2).$$

Then, for the measurement (21) *it follows that*

$$0 = \theta(x_1, x_2, 1) = Z_{0,0}(1) + \sum_{(n,m)\in\mathbb{N}^2\setminus(0,0)}^{\infty} \frac{B_{n,m}\rho_{n,m}(1)\omega_{n,m}}{a_1^2 + 4\omega_{n,m}^2}\cos(n\pi x_1)\cos(m\pi x_2).$$

This yields that $B_{n,m} = 0$, $\forall (n,m) \in \mathbb{N}^2 \setminus (0,0)$. *Then,* $Z_{0,0}(1) = 0$ *which implies* $B_{0,0} = 0$ *since the function* $(e^z - 1)/z$ *is strictly increasing and positive for* $z \in \mathbb{R}_-$.

Similarly, for the time-average measurement it yields that $B_{n,m} = 0$, $\forall n, m \in \mathbb{N}$. *Therefore, under assumption* (18) *the uniqueness of solution for the Neumann problem also holds.*

Remark 2.2. *In* $d = 1$, *one-dimension with* $\Omega = [0, L_1]$, *the problem* (8)–(10) *and* (17), *simplifies to*

$$\frac{\partial^2\theta}{\partial t^2} + a_1\frac{\partial\theta}{\partial t} = a_2\frac{\partial^2\theta}{\partial x^2} - a_4(\theta - \theta_a) + F(x), \quad x \in (0,1),\ t \in (0,1], \tag{32}$$

subject to the initial conditions

$$\theta(x,0) = 0, \quad \frac{\partial\theta}{\partial t}(x,0) = 0, \quad x \in [0,1], \tag{33}$$

and the Dirichlet boundary condition

$$\theta(x,t) = f(x,t), \quad (x,t) \in \{0,1\} \times (0,1], \tag{34}$$

where

$$a_1 = \frac{t_f}{\overline{\tau}} + \frac{w_b C_b t_f}{C_{\mathrm{t}}}, \quad a_2 = \frac{k t_f^2}{\overline{\tau} C_{\mathrm{t}} L_1^2}, \quad a_4 = \frac{w_b C_b t_f^2}{\overline{\tau} C_{\mathrm{t}}}, \tag{35}$$

and we have re-denoted x_1 *by* x. *Also, the condition* (18) *simplifies to*

$$\frac{|C_{\mathrm{t}} - w_b C_b \overline{\tau}|}{\sqrt{\overline{\tau} C_{\mathrm{t}} k}} < \frac{2\pi}{L_1}. \tag{36}$$

Although, as seen in Theorem 2.1, a solution to the IP1 (and IP2) is unique, these problems are still ill-posed since the continuous dependence upon the data (stability) is violated. This can be seen from the following example.

Example of instability. For each $n \in \mathbb{N}^*$, consider the IP1 given by

$$\begin{aligned}
&\theta_{tt} + a_1\theta_t = a_2\theta_{xx} - a_4\theta + F(x), \quad x \in (0,1),\ t \in (0,1],\\
&\theta(x,0) = \theta_t(x,0) = 0, \quad x \in [0,1],\\
&\theta(0,t) = \theta(1,t) = 0, \quad t \in (0,1],\\
&\theta(x,1) = \theta_{1n}(x) = \left[e^{-a_1/2}\left(\cos(\beta_n) + \frac{a_1}{2\beta_n}\sin(\beta_n)\right) - 1\right]\frac{\zeta_n \sin(n\pi x)}{a_4 + a_2 n^2\pi^2}, \quad x \in (0,1),
\end{aligned}$$

where $\beta_n = \dfrac{\sqrt{4(a_4 + a_2 n^2\pi^2) - a_1^2}}{2}$ and ζ_n is yet to be prescribed. Assuming that the condition (18) holds it follows that β_n is a well-defined positive real number. Then, one can easily derive/check that the above problem has a unique solution given by

$$\theta_n(x,t) = \left[e^{-a_1 t/2}\left(\cos(\beta_n t) + \frac{a_1}{2\beta_n}\sin(\beta_n t)\right) - 1\right]\frac{\zeta_n \sin(n\pi x)}{a_4 + a_2 n^2\pi^2}, \quad x \in (0,1),\ t \in (0,1], \tag{37}$$

and

$$F_n(x) = -\zeta_n \sin(n\pi x), \quad x \in [0,1]. \tag{38}$$

As in [8], on choosing, $\zeta_n = \sqrt{n}$, a sequence of source solutions F_n is obtained whose $L^2(0,1)$-norms tend to infinity, while the data $\theta_{1n}(x)$ tends to zero uniformly, as $n \to \infty$. On the other hand, on choosing, $\zeta_n = 1$, a sequence of source solutions F_n is obtained whose $L^2(0,1)$-norms remain constant, while the data $\theta_{1n}(x)$ tends again to zero uniformly, as $n \to \infty$.

A similar example can be constructed for the IP2 by integrating with respect to t expression (37) and remarking that the obtained data $\Theta_{1n}(x)$ tends to zero uniformly, as $n \to \infty$.

The above analysis shows that the IP1 (and IP2) does not depend continuously on the input data, hence they are ill-posed.

3. Variational problems

To solve the IP1 or IP2, we minimize the least-squares objective functionals defined by:

$$J_1(F) := \frac{1}{2}\left\|\theta(\mathbf{x},1) - \theta_1^\epsilon(\mathbf{x})\right\|^2, \tag{39}$$

or

$$J_2(F) := \frac{1}{2}\left\|\int_0^1 \theta(\mathbf{x},t)dt - \Theta_1^\epsilon(\mathbf{x})\right\|^2, \tag{40}$$

where θ solves (7)–(9) for a given source F, θ_1^ϵ and Θ_1^ϵ are noisy perturbations of the exact data (11) and (12), and the norms are in $L^2((0,1)^2)$.

Next, in Theorem 3.1 below, we prove that the objective functional (39) (or (40)) is Fréchet differentiable and derive a formula for its gradient. But before that let us formulate the weak form of the direct problem. Let us denote $D_0 := \{(x_1,x_2) \in (0,1)^2\}$, $D := \{(x_1,x_2,t) | (x_1,x_2) \in D_0,\ t \in (0,1]\}$ and $\Gamma := \{(x_1,x_2,t) | (x_1,x_2) \in \partial D_0,\ t \in [0,1]\}$, and, for simplicity, let us assume that the Dirichlet boundary condition (9) is of the homogeneous form

$$\theta(x_1,x_2,t) = 0, \quad (x_1,x_2,t) \in \Gamma. \tag{41}$$

Then the weak solution $u \in H_0^1(D)$ of the direct problem (8), (17) and (41) satisfies the integral identity

$$\int_D [-\theta_t v_t + \theta(a_4 v - a_1 v_t) + a_2\theta_{x_1}v_{x_1} + a_3\theta_{x_2}v_{x_2}]d\mathbf{x}dt$$

$$= \int_{D_0} F(\mathbf{x}) \left(\int_0^1 v(\mathbf{x}, t) dt \right) d\mathbf{x} + a_4 \int_D \theta_a v d\mathbf{x} dt,$$

for any $v(\mathbf{x}, t) \in H_0^1(D)$ with $v(\cdot, 1)|_{D_0} = 0$, where $H_0^1(D) = \{v \in H^1(D);\ v(\cdot, t)|_{\partial D_0} = 0, \forall t \in (0, 1]\}$. Using the theory of hyperbolic partial differential equations (Chapter IV, Section 3 of [18]), under general regularity on the input data, e.g. $F \in L^2(D_0)$ and $\theta_a \in L^{2,1}(D)$, the above formulation yields a unique solution of the direct problem (8), (17) and (41) satisfying the stability estimate

$$\|u\|_{H^1(D)} + \|u_t\|_{L^2(D)} \leq C(\|F\|_{L^2(D_0)} + \|\theta_a\|_{L^{2,1}(D)}), \tag{42}$$

for some positive constant C. In the above, the space $L^{2,1}(D)$ consists of all elements of $L^1(D)$ with finite norm $\|\theta_a\|_{L^{2,1}(D)} := \int_0^1 \|\theta_a(\cdot, t)\| dt < \infty$.

Theorem 3.1. *The objective functional* (39) *is Fréchet differentiable and its gradient is given by*

$$J_1'(F) = -\int_0^1 v(\mathbf{x}, t) dt, \tag{43}$$

where $\mathbf{x} = (x_1, x_2)$ *in two-dimensions and* $v(x_1, x_2, t)$ *is the solution of the following adjoint problem:*

$$v_{tt} - a_1 v_t = a_2 v_{x_1 x_1} + a_3 v_{x_2 x_2} - a_4 v, \quad (x_1, x_2, t) \in D, \tag{44}$$

$$v(x_1, x_2, 1) = 0, \quad v_t(x_1, x_2, 1) = \theta(x_1, x_2, 1) - \theta_1^\epsilon(x_1, x_2), \quad (x_1, x_2) \in \overline{D_0}, \tag{45}$$

$$v(x_1, x_2, t) = 0, \quad (x_1, x_2, t) \in \Gamma. \tag{46}$$

Proof. Taking a small variation $\Delta F \in L^2(D_0)$ of F, we have

$$J_1(F + \Delta F) - J_1(F) = \left\langle \theta(\mathbf{x}, 1; F) - \theta_1^\epsilon(\mathbf{x}), \Delta\theta(\mathbf{x}, 1; F) \right\rangle_{L^2(D_0)} + \frac{1}{2} \left\| \Delta\theta(\mathbf{x}, 1; F) \right\|_{L^2(D_0)}^2, \tag{47}$$

where $\Delta\theta$ is the solution of the sensitivity problem:

$$(\Delta\theta)_{tt} + a_1(\Delta\theta)_t = a_2(\Delta\theta)_{x_1 x_1} + a_3(\Delta\theta)_{x_2 x_2} - a_4 \Delta\theta + \Delta F, \quad (x_1, x_2, t) \in D, \tag{48}$$

$$\Delta\theta(x_1, x_2, 0) = (\Delta\theta)_t(x_1, x_2, 0) = 0, \quad (x_1, x_2) \in \overline{D_0}, \tag{49}$$

$$(\Delta\theta)(x_1, x_2, t) = 0, \quad (x_1, x_2, t) \in \Gamma. \tag{50}$$

From the *a priori* estimate (42) applied to the sensitivity problem (48)–(50), we have

$$\left| |\Delta\theta(\mathbf{x}, 1; F)| \right|^2 = o\big(\|\Delta F\|\big) \quad \text{as } \|\Delta F\| \to 0. \tag{51}$$

Moreover, multiplying (44) by $\Delta\theta(\mathbf{x}, t)$ and integrating by parts twice, using (45)–(50), yield

$$\int_{(0,1)^2} \big(\theta(\mathbf{x}, 1; F) - \theta_1^\epsilon(\mathbf{x})\big) \Delta\theta(\mathbf{x}, 1; F) d\mathbf{x} = -\int_{(0,1)^2} \left(\int_{(0,1)} v(\mathbf{x}, t) \Delta F(\mathbf{x}) dt \right) d\mathbf{x}. \tag{52}$$

Therefore, equation (47) becomes

$$J_1(F+\Delta F)-J_1(F)=-\int_{(0,1)^2}\left(\int_{(0,1)} v(\mathbf{x},t)\Delta F(\mathbf{x})dt\right)d\mathbf{x}+o\big(\|\Delta F\|\big). \tag{53}$$

From the right-hand side of the above equation and the definition of the Fréchet derivative, we see that J_1 is Fréchet differentiable and its gradient at F is given by (43).

Remark 3.1. *The objective functional $J_2(F)$ of the IP2 is Fréchet differentiable and its gradient is given by*

$$J_2'(F)=-\int_0^1 V(\mathbf{x},t)dt, \tag{54}$$

where $V(\mathbf{x},t)$ is the solution of the following adjoint problem:

$$V_{tt}-a_1V_t=a_2V_{x_1x_1}+a_3V_{x_2x_2}-a_4V,\quad (x_1,x_2,t)\in D, \tag{55}$$

$$V(x_1,x_2,1)=0,\quad V_t(x_1,x_2,1)=\int_0^1\theta(x_1,x_2,t)dt-\Theta_1^\epsilon(x_1,x_2),\quad (x_1,x_2)\in\overline{D_0}, \tag{56}$$

$$V(x_1,x_2,t)=0,\quad (x_1,x_2,t)\in\Gamma. \tag{57}$$

The next subsection describes the CGM utilized for the minimization of the objective functional J_1 given by (39) (or J_2 given by (40)).

3.1 Iterative procedure

The CGM is utilized to reconstruct the unknown space-dependent source F in equation (7) by minimizing the objective functional J, where J stands for J_1 or J_2. The iterative CGM procedure reads:

$$F^{n+1}(\mathbf{x})=F^n(\mathbf{x})-\alpha_nP_n(\mathbf{x}),\quad n=0,1,2,\dots \tag{58}$$

where the direction of descent P_n is given by

$$P_n(\mathbf{x})=\begin{cases}-J'(F^n), & \text{if } n=0,\\ -J'(F^n)+\beta_nP_{n-1}, & \text{if } n=1,2,\dots,\end{cases} \tag{59}$$

the Fletcher–Reeves conjugate coefficient β_n is given by

$$\beta_0=0,\qquad \beta_n=\frac{\|J'(F^n)\|^2}{\|J'(F^{n-1})\|^2},\quad n=1,2,\dots, \tag{60}$$

and the search step size α_n is computed as the minimizer

$$\alpha_n=\underset{\alpha\geq 0}{\operatorname{argmin}}\ J(F^n-\alpha P_n),\quad n=0,1,\dots. \tag{61}$$

For IP1, following the rule (61), we have

$$J_1(F^n - \alpha P_n) = \frac{1}{2}\left\|\theta(\mathbf{x}, 1; F^n - \alpha P_n) - \theta_1^\epsilon(\mathbf{x})\right\|^2. \tag{62}$$

We set $\Delta F^n = P_n$ and linearize $\theta(\mathbf{x}, 1; F^n - \alpha P_n)$ by a first-order Taylor series expression to obtain

$$\theta(\mathbf{x}, 1; F^n - \alpha P_n) \approx \theta(\mathbf{x}, 1; F^n) - \alpha P_n \frac{\partial \theta}{\partial F^n}(\mathbf{x}, 1; F^n) \approx \theta(\mathbf{x}, 1; F^n) - \alpha \Delta\theta(\mathbf{x}, 1; F^n), \tag{63}$$

where $\Delta\theta(\mathbf{x}, 1; F^n)$ is found by solving the sensitivity problem (48)–(50) with $\Delta F^n = P_n$. Then, differentiating $J_1(F^n - \alpha P_n)$ with respect to α and making it zero yield

$$\alpha_n = \frac{\left\langle \theta(\mathbf{x}, 1; F^n) - \theta_1^\epsilon(\mathbf{x}), \Delta\theta(\mathbf{x}, 1; F^n) \right\rangle}{\left\|\Delta\theta(\mathbf{x}, 1; F^n)\right\|^2}. \tag{64}$$

The search step size α_n for IP2 can be obtained by the same method and it is given by

$$\alpha_n = \frac{\left\langle \int_0^1 \theta(\mathbf{x}, t; F^n)dt - \Theta_1^\epsilon(\mathbf{x}), \int_0^1 \Delta\theta(\mathbf{x}, t; F^n)dt \right\rangle}{\left\| \int_0^1 \Delta\theta(\mathbf{x}, t; F^n)dt \right\|^2}. \tag{65}$$

3.2 Stopping criterion

Because the inverse source problems at hand are ill-posed, the CGM is unstable, i.e. small errors in the input data (11) or (12) lead to large errors in the output source solution F. Therefore, we restore stability by stopping the iterations according to the discrepancy principle, i.e. we stop the iterations at the first iteration n_* for which the following stopping criterion is satisfied:

$$J(F^{n_*}) \approx \bar{\epsilon}, \tag{66}$$

where $\bar{\epsilon}$ is a small positive value, e.g. $\bar{\epsilon} = 10^{-5}$, for exact data or

$$\bar{\epsilon} = \frac{1}{2}||Y - Y^{\text{exact}}||, \tag{67}$$

for noisy data, where J and Y mean J_1 and θ_1^ϵ or J_2 and Θ_1^ϵ for IP1 and IP2, respectively.

3.3 Algorithm

The CGM's steps for IP1 (and similarly for IP2) are described as follows:

1. Set $n = 0$ and select an arbitrary initial guess $F^0 \in L^2((0,1)^2)$.
2. Solve the direct problem given by equations (7)–(9) to obtain $\theta(\mathbf{x}, t; F^n)$ and compute $J_1(F^n)$ from equation (39).
3. Stop if the stopping criterion (66) is satisfied. Else go to step 4.

4. Solve the adjoint problem given by equations (44)–(46) to find $v(\mathbf{x}, t; F^n)$. Compute the gradient $J_1'(F^n)$ from equation (43), the conjugate coefficient β_n from equation (60), and the direction of descent P_n from equation (59).

5. Solve the sensitivity problem given by equations (48)–(50) to obtain $\Delta\theta(\mathbf{x}, t; F^n)$ by taking $\Delta F^n = P_n$ and compute the search step size α_n from equation (64).

6. Update F^{n+1} from equation (58), set $n = n + 1$ and go to step 2.

4. Numerical results and discussion

The direct, adjoint and sensitivity problems present in the CGM described in Section 3.3 are solved using the Crank-Nicolson scheme [10], in one-dimension ($d = 1$) with uniform mesh size $\Delta x = 1/M^{(1)}$ and time step $\Delta t = 1/N$, or the alternating direction implicit (ADI) scheme [5], relying on the Peaceman-Rachford splitting strategy in two-dimensions ($d = 2$) with mesh sizes $\Delta x_1 = 1/M^{(1)}$ and $\Delta x_2 = 1/M^{(2)}$, and time step $\Delta t = 1/N$. The trapezoidal rule is used for discretizing all the integrals in this paper, e.g. the objective functionals (39) and (40). The measurements θ_1 and Θ_1 are generated numerically by solving the direct problem (7)–(9) using the aforementioned finite-difference methods with $M^{(1)} = N = 80$ in $d = 1$ or $M^{(1)} = M^{(2)} = N = 80$ in $d = 2$. Moreover, to avoid committing an inverse crime we employ half the mesh sizes used to generate θ_1 and Θ_1 when solving the inverse problems. The noisy data θ_1^ϵ and Θ_1^ϵ are simulated by adding random noise to the noise-free data θ_1 and Θ_1, as follows:

$$\theta_1^\epsilon = \theta_1 + \epsilon p \max|\theta_1|, \quad \Theta_1^\epsilon = \Theta_1 + \epsilon p \max|\Theta_1|, \tag{68}$$

where p represents the percentage of noise and ϵ are random variables generated from a Gaussian normal distribution with mean 0 and variance 1 using the MATLAB command $randn(size(\theta_1))$ or $randn(size(\Theta_1))$.

The accuracy error functional, as a function of the number of iterations n, is defined as:

$$E(F^n) = \|F^n - F\|, \tag{69}$$

where F^n denotes the numerical result obtained by the CGM at the iteration number n and F stands for the exact source, if available.

We finally mention that the dimensional source Q_e in (1) is obtained via (6) after F has been reconstructed.

4.1 Example 1 (exponential-type source)

We first consider the model (1)–(3) for heat transfer in tissues radiated by an electromagnetic antenna during thermal therapy in one-dimension $d = 1$ on $\Omega = [0, L_1]$ with the physical parameters taken from [1, 16, 25] as

$$k = 0.5 \text{ W/(m °C)}, \ \rho_t = \rho_b = 1050 \text{ kg/m}^3, \ c_t = c_b = 3800 \text{ J/(kg °C)}, \ w_b = 0.04 \text{ s}^{-1}, \tag{70}$$

$$\overline{\tau} = 20 \text{ s},\ T_a = T_0 = \text{f} = 37^{\circ}\text{C},\ L_1 = 0.05 \text{ m},\ t_{\text{f}} = 60 \text{ s},\ Q_m = 0, \tag{71}$$

and the following source taken from [16] as

$$Q_e(\bar{x}) = \rho_{\text{t}} \kappa \Lambda_0 e^{a(\bar{x}-0.01)}, \quad \bar{x} \in [0, L_1], \tag{72}$$

where $\kappa = 12.5 \text{ kg}^{-1}$ and $a = -127 \text{ m}^{-1}$ are the antenna constants, and $\Lambda_0 = 1$ W is the transmitted power. One can easily check that condition (36) with the above parameters is marginally violated. However, as the numerical investigation below will indicate, the uniqueness of solution seems to hold for Example 1 (and also for Examples 2 and 3) even when the sufficient condition (36) for uniqueness is violated.

Equivalent to the one-dimensional version of (1)–(3) we consider (32)–(34) with the following parameters obtained via (6), (35) and (70)–(72) as

$$a_1 = 5.4,\ a_2 = 9.0226 \times 10^{-3},\ a_4 = 7.2,\ \tau = 0.3333,\ \theta_a = V_0 = f = 0, \tag{73}$$

$$F(x) = 1.6003 \times 10^{-2} e^{-6.35x+1.27}, \quad x \in [0, 1]. \tag{74}$$

We employ the CGM described in Section 3.3 to minimize the objective functionals (39) and (40) starting from the initial guess given as the linear interpolant of (74) at the boundary $x \in \{0, 1\}$, namely,

$$F^0(x) = -0.0569x + 0.057, \quad x \in [0, 1]. \tag{75}$$

Figures 1(a) and 2(a) show the monotonic decreasing convergence of the objective functionals (39) and (40) that are minimized for IP1 and IP2, respectively, as functions of the number of iterations n, for $p \in \{0, 5\%, 20\%\}$ noise. For exact data, i.e. $p = 0$ in (68), the objective functionals (39) and (40) rapidly attain very low values of $\mathcal{O}(10^{-12})$ and $\mathcal{O}(10^{-14})$, respectively, and we stop the iterative process after 10 iterations. For noisy data $p \in \{5, 20\}\%$, the stopping iteration numbers $n_* \in \{1, 1\}$ are chosen according to the discrepancy principle (66). The error curves (69) for IP1 and IP2, as functions of the number of iterations n, are depicted in Figures 1(b) and 2(b), and the numerical solutions for the source Q_e are displayed in Figures 1(c) and 2(c) alongside the exact source (72). The errors (69) of the numerical solutions for IP1 and IP2 are shown in Table 1. From these results, it can be seen that the numerical solutions agree very well with the exact source (72) in the case of noise-free data. Furthermore, in the case of noisy data, it can be concluded that the numerical solutions are accurate and reasonably stable and they become more accurate as the percentage of noise p decreases.

4.2 Example 2 (Gaussian-type source)

In this example, the model (1)–(3) in one-dimension $d = 1$ on $\Omega = [0, L_1]$ is considered with the parameters (70), (71) and the following source taken from [17] as

$$Q_e(\bar{x}) = Q_{e0} e^{-a_0^2(\bar{x}-0.025)^2}, \quad \bar{x} \in [0, L_1], \tag{76}$$

where $Q_{e0} = 7.58 \times 10^3$ W/m^3 is a reference heat source and $a_0 = 100 \text{ m}^{-1}$ is the scattering parameter.

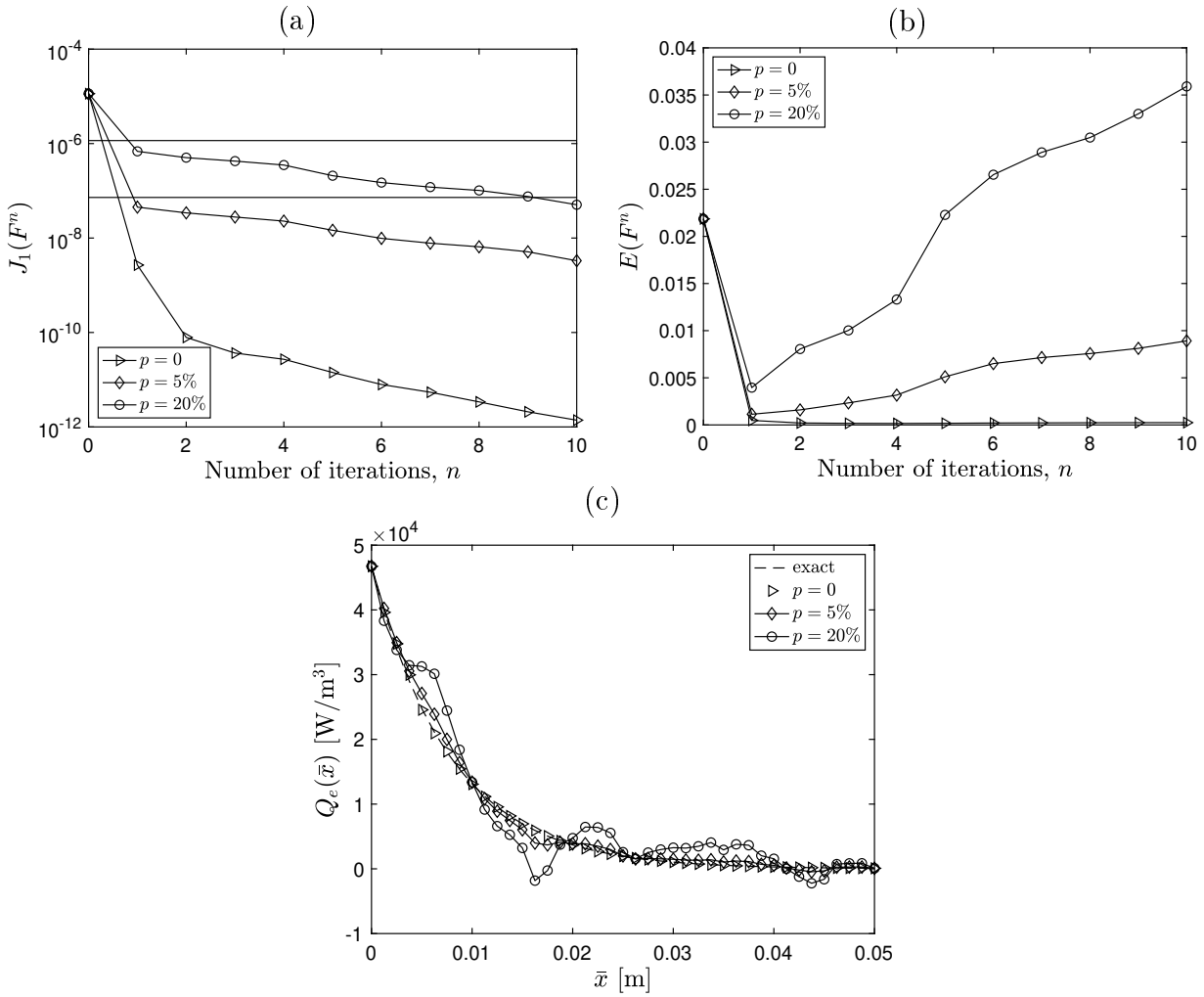

Figure 1: The objective functional (a) given by (39), (b) the error (69), and (c) the exact (72) and numerical source $Q_e(\bar{x})$, for $p \in \{0, 5\%, 20\%\}$ noise, for Example 1.

Table 1: The error (69) of the numerical solutions for IP1 and IP2 of Examples 1–4.

p	Example 1		Example 2		Example 3		Example 4	
	IP1	IP2	IP1	IP2	IP1	IP2	IP1	IP2
0	2.4E–4	2.4E–4	7.2E–7	1.1E–6	7.3E–11	6.1E–11	3.1E–3	3.3E–3
5%	1.1E–3	1.1E–3	2.2E–4	2.5E–4	7.7E–10	8.7E–10	1.5E–2	1.5E–2
20%	4.0E–3	3.6E–3	8.3E–4	8.5E–4	2.7E–9	3.1E–9	4.4E–2	4.1E–2

Equivalent to (1)–(3) in one-dimension $d = 1$, we consider (32)–(34) with the parameters (73) and the source obtained via (6), (70), (71) and (76) as

$$F(x) = 9.242 \times 10^{-3} e^{-25(x-0.5)^2}, \quad x \in [0, 1]. \tag{77}$$

The CGM described in Section 3.3 is employed to minimize the objective functionals

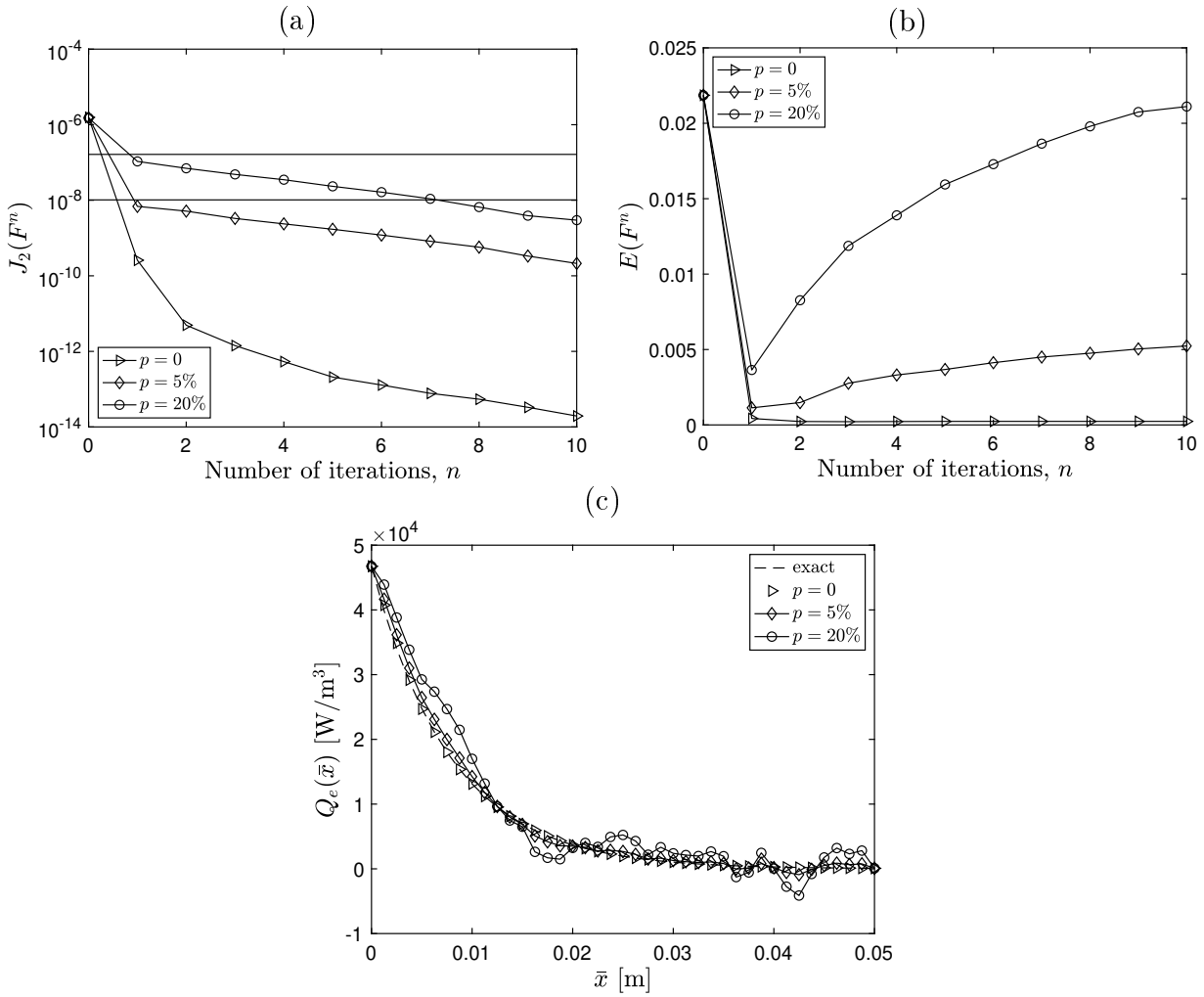

Figure 2: The objective functional (a) given by (40), (b) the error (69), and (c) the exact (72) and numerical source $Q_e(\bar{x})$, for $p \in \{0, 5\%, 20\%\}$ noise, for Example 1.

(39) and (40) starting from the initial guess $F^0(x) = 1.7841 \times 10^{-5}$ for $x \in [0, 1]$, which ensures that $F^0(0) = F(0)$ and $F^0(1) = F(1)$, where F is given by (77).

Figures 3(a) and 4(a) show the monotonic decreasing convergence of the objective functionals (39) and (40) that are minimized for IP1 and IP2, respectively, as functions of the number of iterations n, for $p \in \{0, 5\%, 20\%\}$ noise. For exact data, i.e. $p = 0$ in (68), the objective functionals (39) and (40) rapidly attain very low values of $\mathcal{O}(10^{-19})$ and we stop the iterative process after 10 iterations. For noisy data $p \in \{5, 20\}\%$, the stopping iteration numbers $n_* \in \{1, 1\}$ are chosen according to the discrepancy principle (66). The error curves (69) for IP1 and IP2, as functions of the number of iterations n, are shown in Figures 3(b) and 4(b), and the numerical solutions for the source Q_e are displayed in Figures 3(c) and 4(c) along with the exact source (76). The errors (69) of the numerical solutions for IP1 and IP2 are presented in Table 1. Conclusions identical to these reported for Example 1 can be drawn for Example 2.

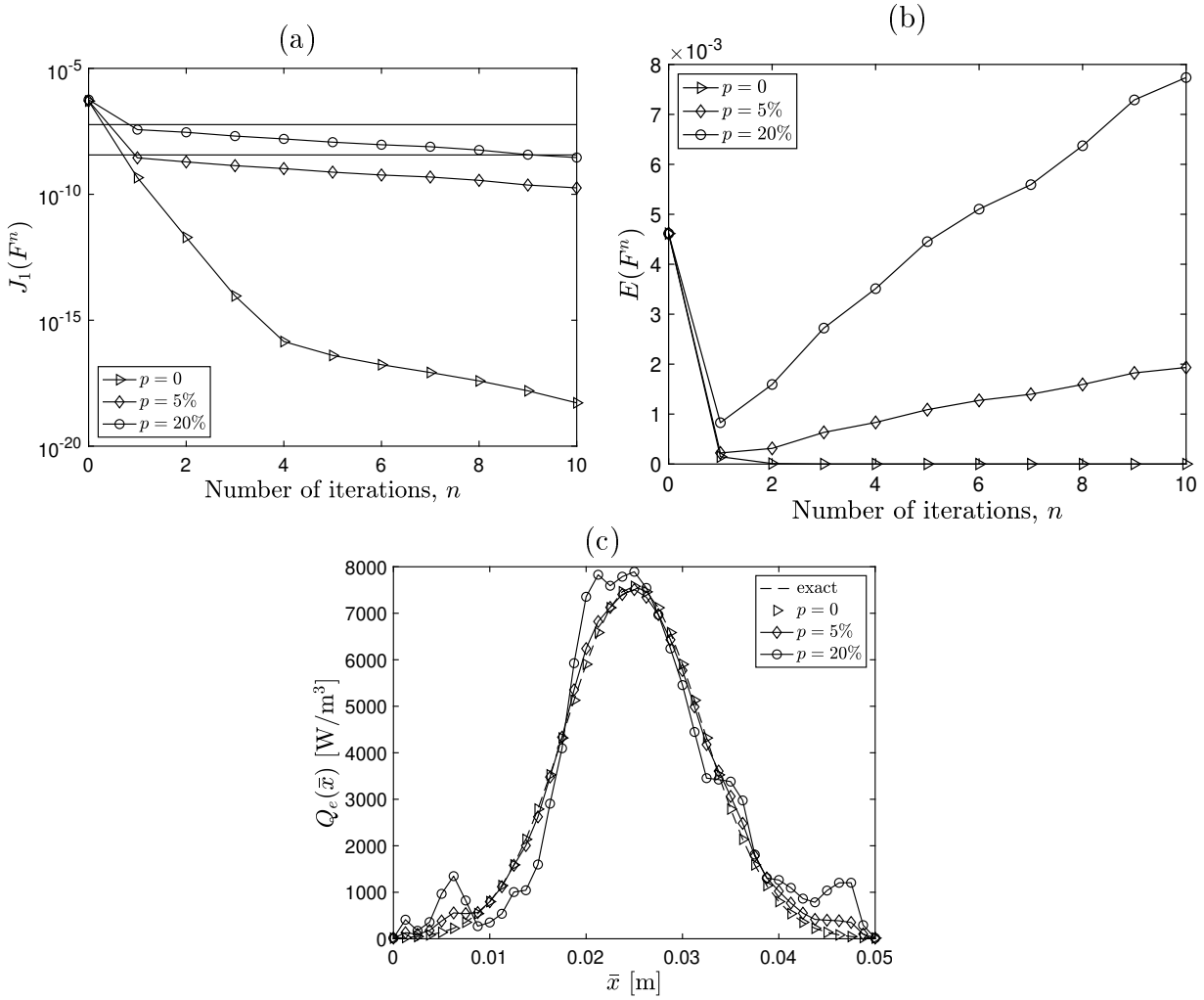

Figure 3: The objective functional (a) given by (39), (b) the error (69), and (c) the exact (76) and numerical source $Q_e(\bar{x})$, for $p \in \{0, 5\%, 20\%\}$ noise, for Example 2.

4.3 Example 3 (piecewise smooth source)

As in Examples 1 and 2, in this example we consider (1)–(3) in one-dimension $d = 1$ on $\Omega = [0, L_1]$ with the parameters (70), (71), and the following piecewise smooth and continuous source

$$Q_e(\bar{x}) = \begin{cases} \bar{x}, & 0 \le \bar{x} \le 0.5L_1, \\ L_1 - \bar{x}, & 0.5L_1 < \bar{x} \le L_1. \end{cases} \tag{78}$$

Equivalent to (1)–(3) in one-dimension $d = 1$, we consider (32)–(34) with the parameters (73) and the source obtained via (6), (70), (71) and (78) as

$$F(x) = \begin{cases} 6.0963 \times 10^{-8} x, & 0 \le x \le 0.5, \\ 6.0963 \times 10^{-8}(1 - x), & 0.5 < x \le 1. \end{cases} \tag{79}$$

We invoke the CGM described in Section 3.3 to minimize the objective functionals

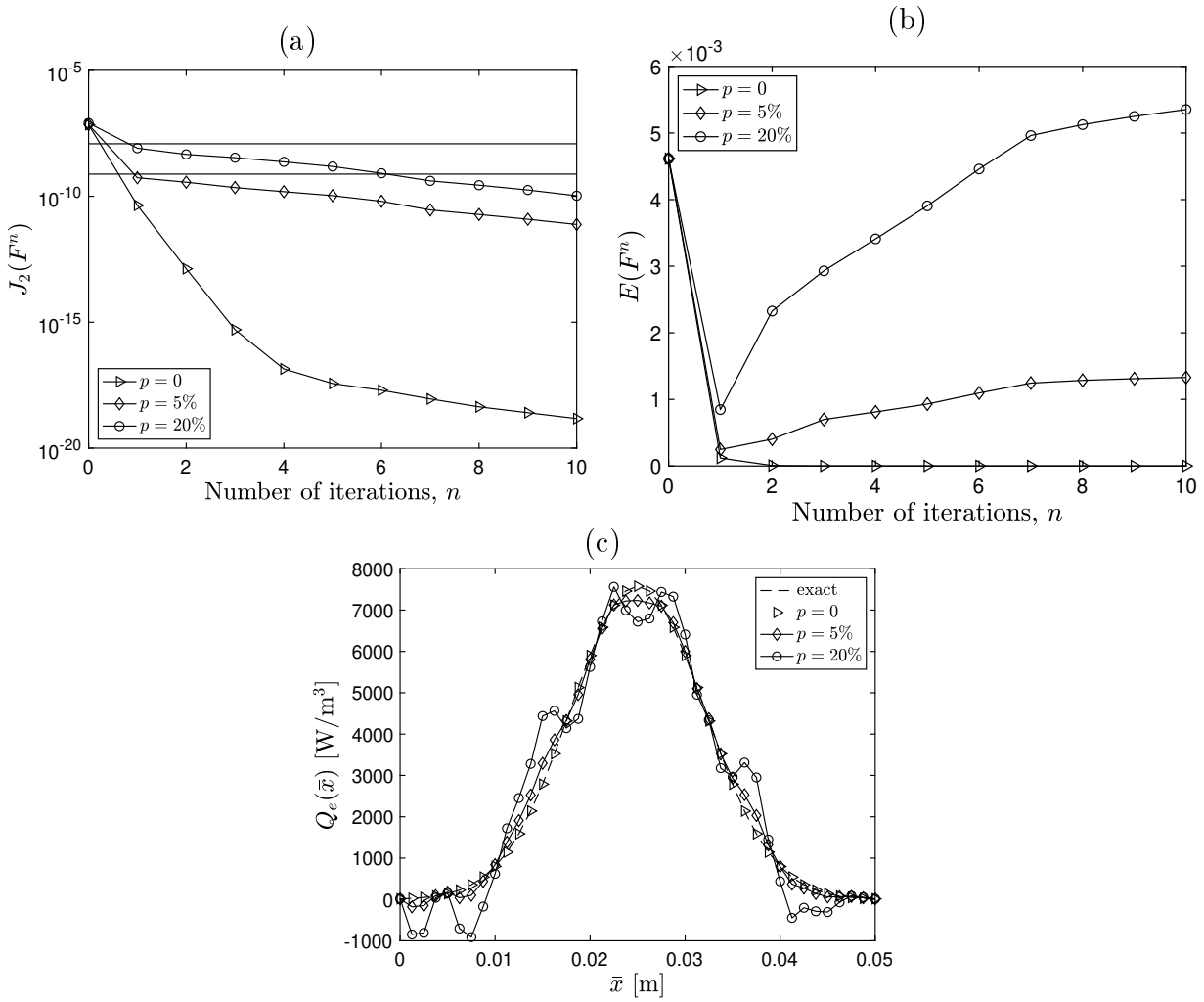

Figure 4: The objective functional (a) given by (40), (b) the error (69), and (c) the exact (76) and numerical source $Q_e(\bar{x})$, for $p \in \{0, 5\%, 20\%\}$ noise, for Example 2.

(39) and (40) starting from the initial guess $F^0(x) = 0$ for $x \in [0, 1]$, which ensures that $F^0(0) = F(0)$ and $F^0(1) = F(1)$, where F is given by (79).

Numerical results and errors displayed in Table 1 as well as Figures 5 and 6 illustrate the same conclusions as these reported for Examples 1 and 2.

4.4 Example 4 (two-dimensional source)

In this final example, we consider equations (1)–(3) on the rectangular domain $\Omega = [0, L_1] \times [0, L_2]$ with the parameters given by (70), (71) and $L_2 = 0.025$ m. The external heat source is taken from [15] as

$$Q_e(\bar{x}_1, \bar{x}_2) = \rho_t \kappa \Lambda_0 \exp\big(a(\bar{x}_1 - 0.01)\big) \exp\left(\frac{b\bar{x}_2^2}{\bar{x}_1 + c}\right), \quad (\bar{x}_1, \bar{x}_2) \in [0, L_1] \times [0, L_2], \tag{80}$$

where $\kappa = 12.5$ kg^{-1}, $a = -127$ m^{-1}, $b = -129$ m^{-1} and $c = 0.0245$ m are antenna constants, and $\Lambda_0 = 20$ W is the transmitted power. One can easily check that condition (18)

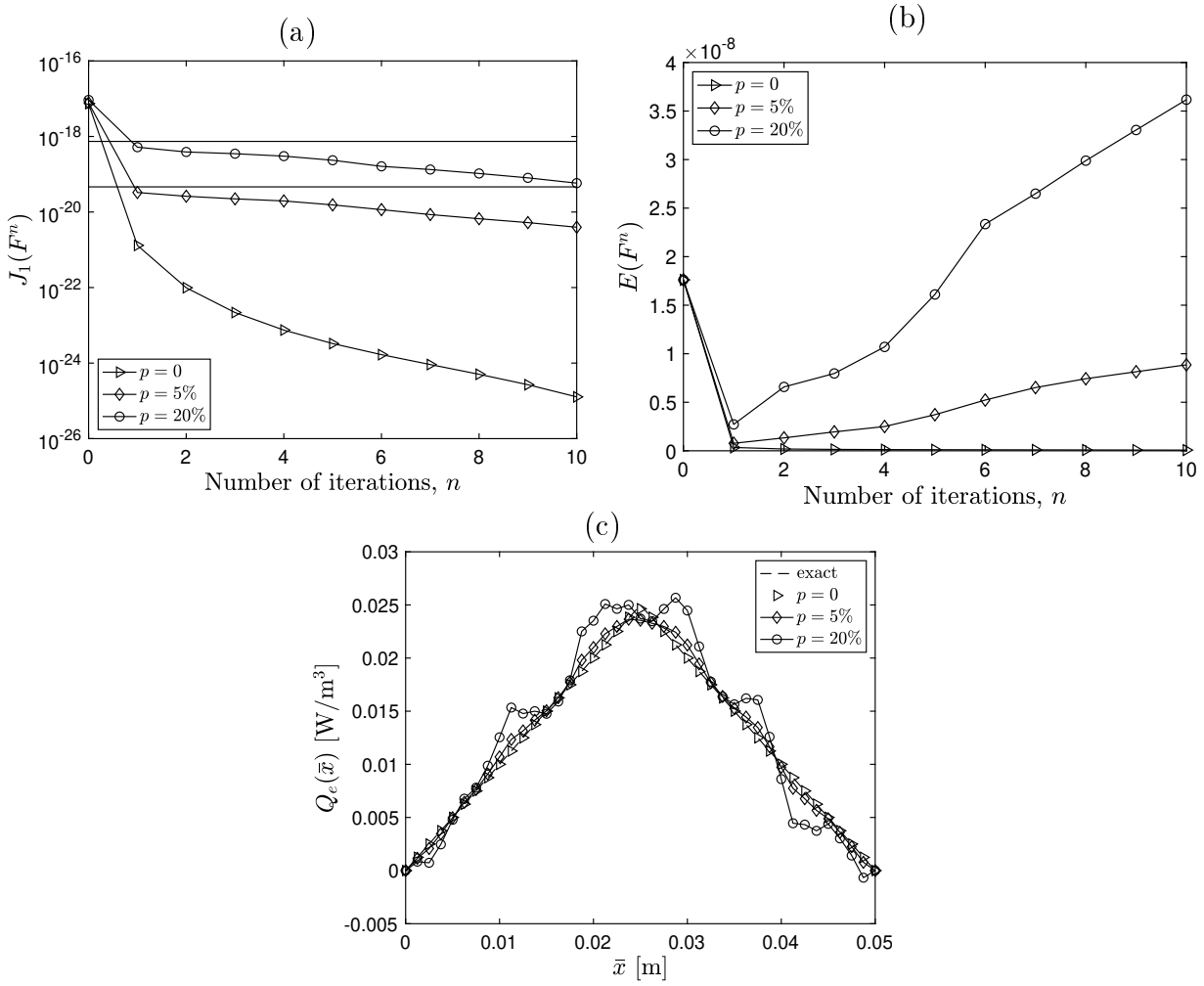

Figure 5: The objective functional (a) given by (39), (b) the error (69), and (c) the exact (78) and numerical source $Q_e(\bar{x})$, for $p \in \{0, 5\%, 20\%\}$ noise, for Example 3.

with the chosen parameters is satisfied such that the uniqueness of solution of the inverse source problems IP1 and IP2 holds.

As before, equivalent to (1)–(3) we consider (7)–(9) with the following parameters obtained via (6), (10), (70), (71) and (80) as

$$a_1 = 5.4,\ a_2 = 9.0226 \times 10^{-3},\ a_3 = 3.609 \times 10^{-2},\ a_4 = 7.2,\ \tau = 0.3333, \tag{81}$$

$$\theta_a = f = 0, \tag{82}$$

$$F(x_1, x_2) = 3.2006 \times 10^{-1} \exp(-6.35x_1 + 1.27) \exp\left(\frac{-1.6125x_2^2}{x_1 + 0.49}\right), \quad (x_1, x_2) \in [0, 1]^2. \tag{83}$$

We run the CGM described in Section 3.3 to minimize the objective functionals (39) and (40) starting from initial guess

$$F^0(x_1, x_2) = F(x_1, x_2) + 100x_1x_2(1 - x_1)(1 - x_2), \quad (x_1, x_2) \in [0, 1]^2, \tag{84}$$

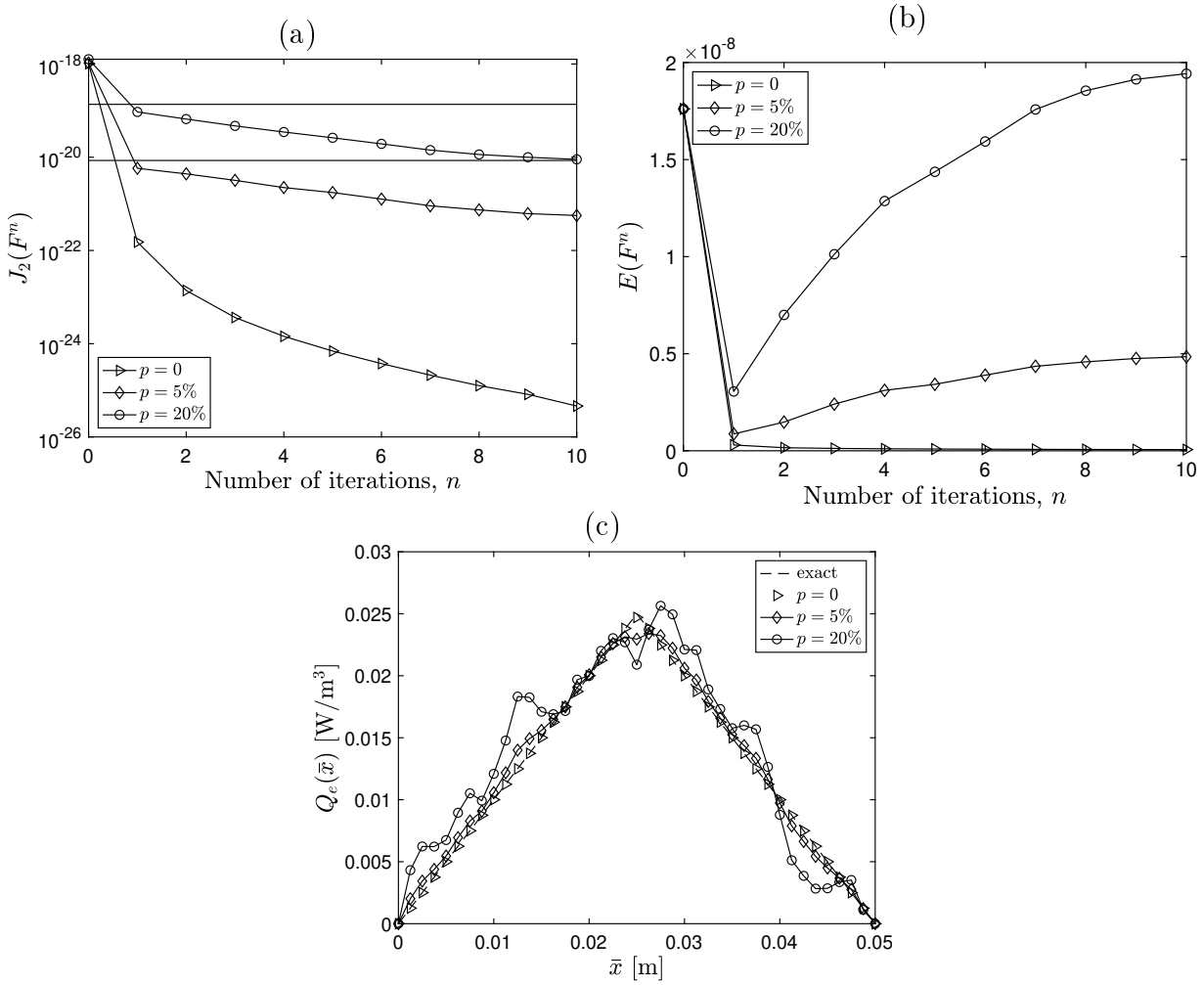

Figure 6: The objective functional (a) given by (40), (b) the error (69), and (c) the exact (78) and numerical source $Q_e(\bar{x})$, for $p \in \{0, 5\%, 20\%\}$ noise, for Example 3.

which ensures that on the boundary $\partial[0,1]^2$, F^0 is equal to the exact source (83).

Figures 7(a) and 9(a) demonstrate the monotonic decreasing convergence of the objective functionals (39) and (40) that are minimized for IP1 and IP2, respectively, as functions of the number of iterations n, for $p \in \{0, 5\%, 20\%\}$ noise. For exact data, i.e. $p = 0$ in (68), the objective functionals (39) and (40) rapidly attain very low values of $\mathcal{O}(10^{-10})$, and we stop the iterative process after 10 iterations. For noisy data $p \in \{5, 20\}\%$, the stopping iteration numbers $n_* \in \{2, 1\}$ are obtained according to the discrepancy principle (66). The error curves (69) for IP1 and IP2, as functions of the number of iterations n, are shown in Figures 7(b) and 9(b), respectively. Moreover, the errors (69) of the numerical solutions for IP1 and IP2 are displayed in Table 1.

Figure 8 and 10 depict the corresponding numerical identifications of the source Q_e in comparison with the exact source (80). Concluding remarks analogous to those of previous examples can be drawn for Example 4.

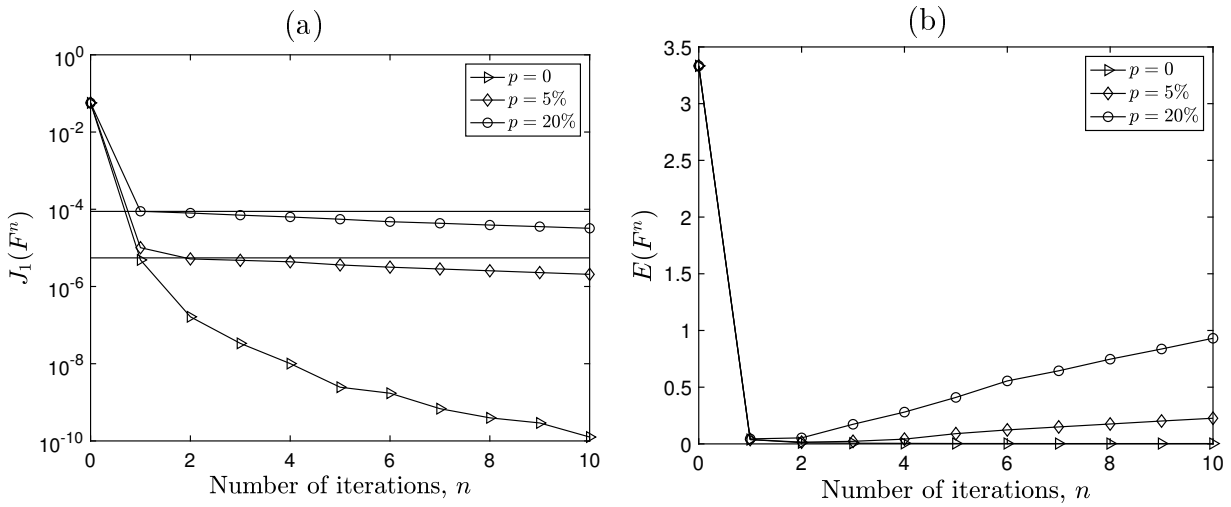

Figure 7: The objective functional (a) given by (39) and (b) the error (69), for $p \in \{0, 5\%, 20\%\}$ noise, for Example 4.

5. Conclusions

This paper has considered the inverse problems of identifying the unknown space-dependent source in the thermal-wave model of bio-heat transfer from final-time or time-average temperature measurements. First, the uniqueness of the solutions of these inverse source problems has been proved using the separation-of-variables method. Establishing the necessity of condition (18) in the uniqueness Theorem 2.1 remains open for research. Then, the inverse problems have been solved numerically by minimizing the least-squares objective functionals using the CGM combined with the discrepancy principle. To show the accuracy and stability of the numerical results, examples concerning the reconstruction of sources of different forms in one and two dimensions have been presented and thoroughly discussed.

Simultaneous recovery of the space-dependent source and perfusion coefficient in the thermal-wave model of bio-heat transfer can also be attempted using the CGM, but this extension is deferred to future work.

Acknowledgements.
M. Alosaimi would like to thank Taif University in Saudi Arabia and the United Kingdom Saudi Arabian Cultural Bureau (UKSACB) in London for supporting his PhD studies at the University of Leeds. D. Lesnic would like to acknowledge the support of the EPSRC grant EP/W000873/1.

References

[1] A. Alkhwaji, B. Vick, and T. Diller. New mathematical model to estimate tissue blood perfusion, thermal contact resistance and core temperature. *Journal of Biomechanical Engineering-Transactions of the ASME*, 134:081004, 2012.

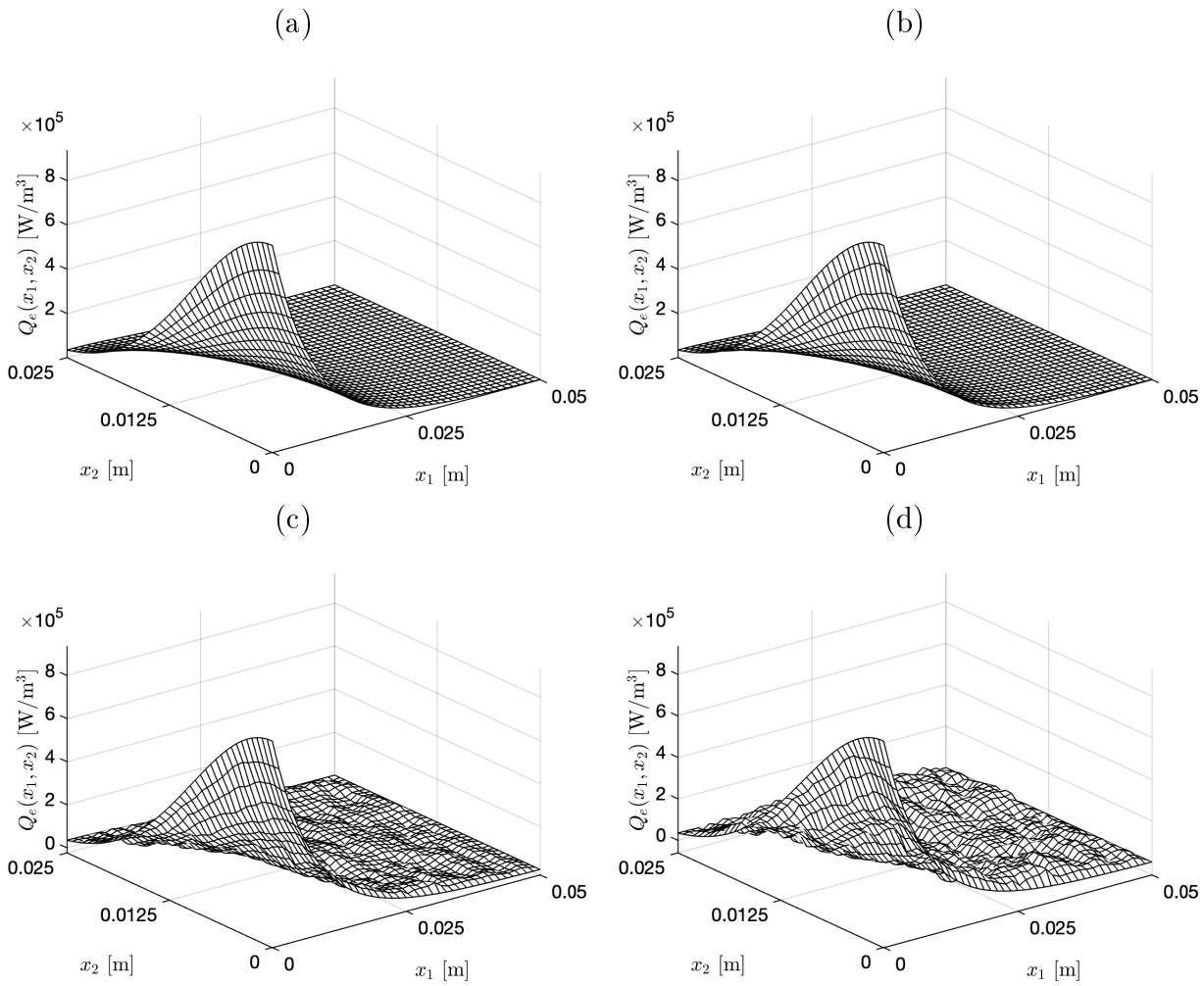

Figure 8: (a) The exact (80) and numerical source $Q_e(\bar{x}_1, \bar{x}_2)$, for (b) $p = 0$, (c) $p = 5\%$ noise, and (d) $p = 20\%$ noise, for IP1 of Example 4.

[2] M. Alosaimi, D. Lesnic, and D. N. Hào. Identification of the forcing term in hyperbolic equations. *International Journal of Computer Mathematics*, 98(9):1877–1891, 2021.

[3] M. Alosaimi, D. Lesnic, and J. Niesen. Determination of the thermo-physical properties of multi-layered biological tissues. *Applied Mathematical Modelling*, 99:228–242, 2021.

[4] M. Alosaimi, D. Lesnic, and J. Niesen. Identification of the thermo-physical properties of a stratified tissue. Adiabatic hypodermic wall. *International Communications in Heat and Mass Transfer*, 126:105376, 2021.

[5] A. Araújo, C. Neves, and E. Sousa. An alternating direction implicit method for a second-order hyperbolic diffusion equation with convection. *Applied Mathematics and Computation*, 239:17–28, 2014.

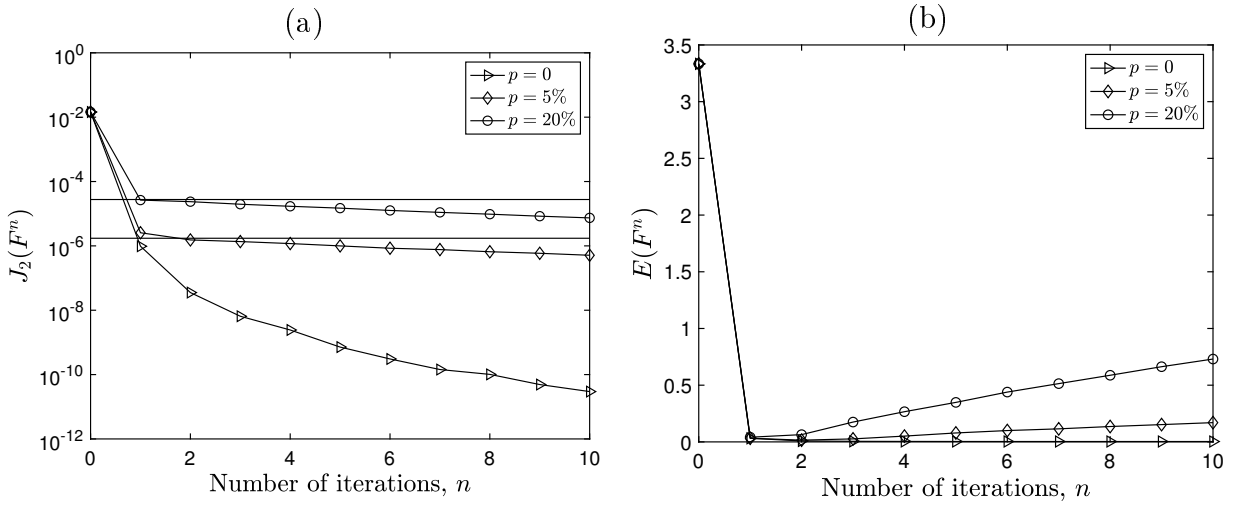

Figure 9: The objective functional (a) given by (40) and (b) the error (69), for $p \in \{0, 5\%, 20\%\}$ noise, for Example 4.

[6] M. Baghban and M. B. Ayani. Source term prediction in a multilayer tissue during hyperthermia. *Journal of Thermal Biology*, 52:187–191, 2015.

[7] F. S. Bazán, L. Bedin, and L. S. Borges. Space-dependent perfusion coefficient estimation in a 2D bioheat transfer problem. *Computer Physics Communications*, 214:18–30, 2017.

[8] J. Cannon and D. Dunninger. Determination of an unknown forcing function in a hyperbolic equation from overspecified data. *Annali di Matematica Pura ed Applicata*, 85(1):49–62, 1970.

[9] K. Cao and D. Lesnic. Reconstruction of the space-dependent perfusion coefficient from final time or time-average temperature measurements. *Journal of Computational and Applied Mathematics*, 337:150–165, 2018.

[10] W. Dai and R. Nassar. A finite difference scheme for solving the heat transport equation at the microscale. *Numerical Methods for Partial Differential Equations*, 15(6):697–708, 1999.

[11] D. N. Hào, B. V. Huong, N. T. N. Oanh, and P. X. Thanh. Determination of a term in the right-hand side of parabolic equations. *Journal of Computational and Applied Mathematics*, 309:28–43, 2017.

[12] D. N. Hào, T. N. T. Quyen, and N. T. Son. Convergence analysis of a Crank–Nicolson Galerkin method for an inverse source problem for parabolic equations with boundary observations. *Applied Mathematics & Optimization*, 84:2289–2325, 2021.

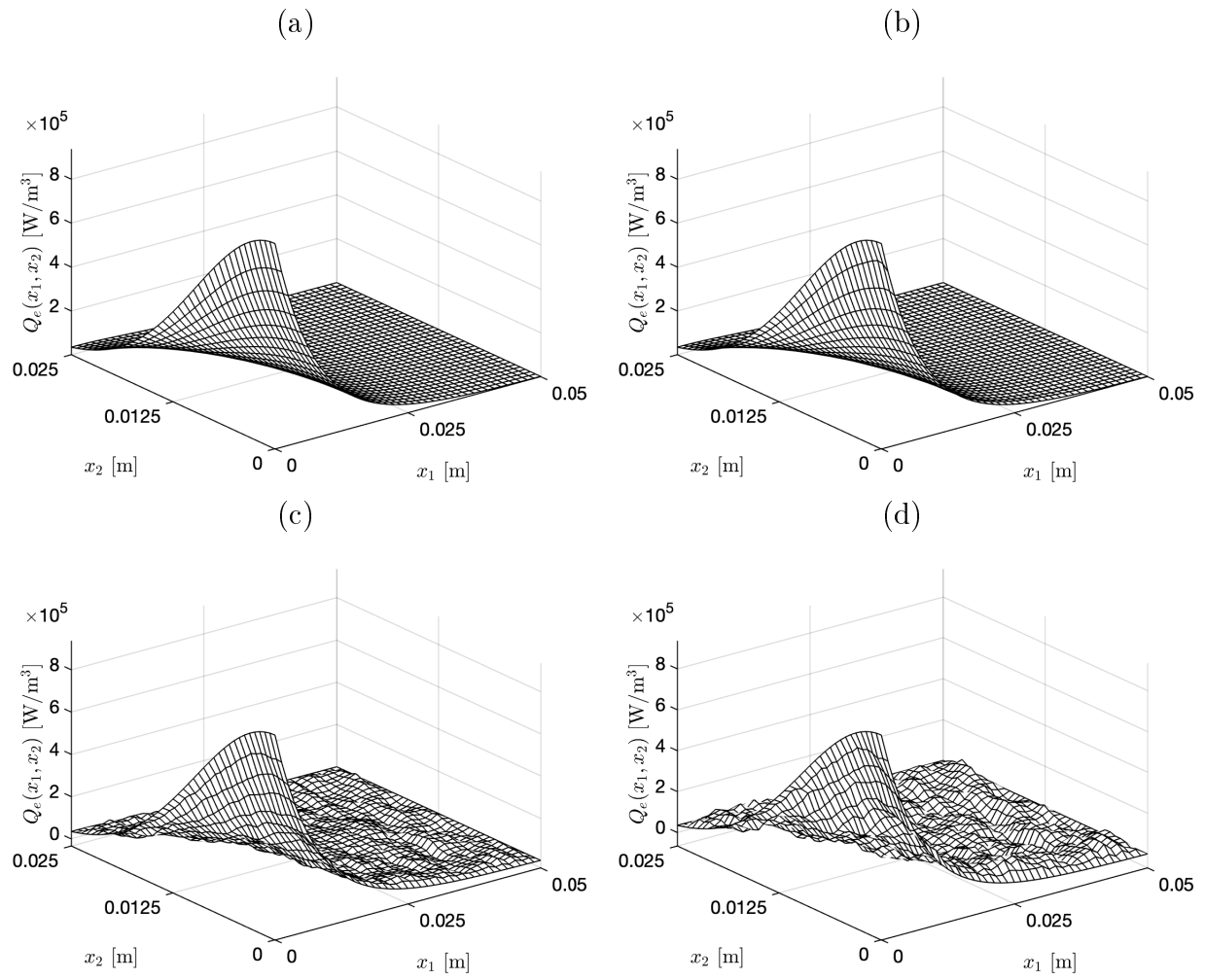

Figure 10: (a) The exact (80) and numerical source $Q_e(\bar{x}_1, \bar{x}_2)$, for (b) $p = 0$, (c) $p = 5\%$ noise, and (d) $p = 20\%$ noise, for the IP2 of Example 4.

[13] A. Hasanov. Simultaneous determination of the source terms in a linear hyperbolic problem from the final overdetermination: weak solution approach. *IMA Journal of Applied Mathematics*, 74(1):1–19, 2009.

[14] A. Jalali, M.-B. Ayani, and M. Baghban. Simultaneous estimation of controllable parameters in a living tissue during thermal therapy. *Journal of Thermal Biology*, 45: 37–42, 2014.

[15] D. Kouremenos and K. Antonopoulos. Heat transfer in tissues radiated by a 432 MHz directional antenna. *International Journal of Heat and Mass Transfer*, 31(10):2005–2012, 1988.

[16] D. Kumar and K. Rai. Numerical simulation of time fractional dual-phase-lag model of heat transfer within skin tissue during thermal therapy. *Journal of Thermal Biology*, 67:49–58, 2017.

[17] R. Kumar, A. K. Vashishth, and S. Ghangas. Variable thermal conductivity approach for bioheat transfer during thermal ablation. *Arab Journal of Basic and Applied Sciences*, 26(1):78–88, 2019.

[18] O. Ladyzhenskaya. *Boundary Value Problems in Mathematical Physics*. Springer, New York, 1985.

[19] D. Lesnic, S. O. Hussein, and B. T. Johansson. Inverse space-dependent force problems for the wave equation. *Journal of Computational and Applied Mathematics*, 306:10–39, 2016.

[20] J. Liu, Z. Ren, and C. Wang. Interpretation of living tissue's temperature oscillations by thermal wave theory. *Chinese Science Bulletin*, 40(17):1493–1495, 1995.

[21] J. Liu, X. Chen, and L. X. Xu. New thermal wave aspects on burn evaluation of skin subjected to instantaneous heating. *IEEE Transactions on Biomedical Engineering*, 46 (4):420–428, 1999.

[22] T. Loulou and E. P. Scott. Thermal dose optimization in hyperthermia treatments by using the conjugate gradient method. *Numerical Heat Transfer: Part A: Applications*, 42(7):661–683, 2002.

[23] F. Maes and M. Slodička. Some inverse source problems of determining a space dependent source in fractional-dual-phase-lag type equations. *Mathematics*, 8(8):1291, 2020.

[24] L. H. Nguyen. An inverse space-dependent source problem for hyperbolic equations and the Lipschitz-like convergence of the quasi-reversibility method. *Inverse Problems*, 35 (3):035007, 2019.

[25] Ş. Özen, S. Helhel, and O. Çerezci. Heat analysis of biological tissue exposed to microwave by using thermal wave model of bio-heat transfer (TWMBT). *Burns*, 34(1): 45–49, 2008.

[26] H. H. Pennes. Analysis of tissue and arterial blood temperatures in the resting human forearm. *Journal of Applied Physiology*, 1(2):93–122, 1948.

[27] V. Romanov and A. Hasanov. Uniqueness and stability analysis of final data inverse source problems for evolution equations. *Journal of Inverse and Ill-Posed Problems*, 30: 425–446, 2022.

[28] J. Singh, P. K. Gupta, and K. N. Rai. Solution of fractional bioheat equations by finite difference method and HPM. *Mathematical and Computer Modelling*, 54(9-10): 2316–2325, 2011.

[29] M. Tunç, Ü. Çamdali, C. Parmaksizoğlu, and S. Çikrikçi. The bio-heat transfer equation and its applications in hyperthermia treatments. *Engineering Computations*, 23:451–463, 2006.